ACS Sustainable Chemistry & Engineering

pubs.acs.org/journal/ascecg

Research Article

Cell Wall Polymer Degradation during *Rhodonia placenta* Brown Rot Decay of Thermally Modified and Unmodified Wood

Tiina Belt,* Muhammad Awais,* Paula Nousiainen, Lauri Rautkari, and Mikko Mäkelä

Cite This: *ACS Sustainable Chem. Eng.* 2025, 13, 17050−17060

Read Online

ACCESS | Metrics & More | Article Recommendations | Supporting Information

ABSTRACT: Thermal modification produces decay-resistant wood suitable for sustainable applications. Although thermally modified wood remains degradable by fungi, its degradation mechanisms are poorly understood, impacting long-term eco-friendly use. This study investigated thermally modified wood degradation by elucidating chemical changes to wood cell wall polymers during *Rhodonia placenta* brown rot decay. Modified and unmodified Scots pine samples were exposed to *R. placenta* in stacked-sample decay tests, generating decay stage progressions. Decayed samples were analyzed by near-infrared spectroscopy with multivariate analysis to identify key chemical changes. Milled wood lignin was isolated and analyzed by two-dimensional nuclear magnetic resonance spectroscopy for further lignin chemistry insight. Results showed that *R. placenta* degraded thermally modified wood to high mass losses. Chemical changes were characterized by carbohydrate degradation and oxidative lignin modification, typical for brown rot. While most degradative changes were similar between modified and unmodified wood, differences in lignin modification patterns were observed. Interestingly, spectroscopic data revealed different chemical changes in the early and late decay stages in modified and unmodified wood. These findings highlight the time-dependent nature of *R. placenta* degradation and show that thermally modified and unmodified woods are degraded by similar yet different mechanisms, providing new insight into brown rot wood degradation.

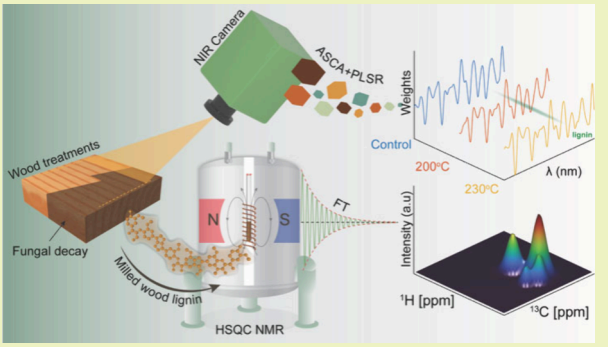

KEYWORDS: *durability, fungal decay, heat treatment, HSQC, lignin modification, NIR, NMR, oxidation*

INTRODUCTION

Wood decaying fungi are highly destructive wood degraders that consume wood cell wall polymers, leading to a loss of material and mechanical strength. Susceptible wood can be protected from decay in many ways, including by using treatments that increase the decay resistance of the material. Wood modification is a term that covers a range of treatments that improve wood properties such as decay resistance using a nontoxic mode of action,[1] offering alternatives to conventional chemical preservatives. Thermal modification is one of the most extensively studied and commercially successful methods that uses thermal degradation rather than chemicals to alter the composition of wood in a sustainable way, leading to improvements in decay resistance and other properties.[2−4]

Thermal modification improves decay resistance by altering the wood cell wall polymers in a way that reduces their hygroscopicity. Hemicelluloses are preferentially degraded and undergo depolymerization as well as deacetylation and dehydration,[5,6] while lignin undergoes cleavage and recondensation, both with itself and with carbohydrate degradation products.[6−8] Hemicelluloses contain more accessible OH groups that are able to participate in sorption than the other wood cell wall polymers,[9] which means that their degradation is expected to reduce hygroscopicity. The reduced hygroscopicity of thermally modified wood is indeed linked to the loss of hemicelluloses and OH groups, but other degradative changes have also been shown to play a substantial role.[10−14] Increased cross-linking, H-bonding networks, hydrophobic substances, and other chemical and structural alterations have been suggested, but the mechanisms behind the hygroscopicity decrease remain poorly understood.[15]

The reduction in hygroscopicity increases the decay resistance of thermally modified wood primarily by decreasing its moisture content, which hinders the diffusion of fungal degradative agents in the cell wall.[16−19] However, even though decay resistance is increased, at least in aboveground applications, the growth of fungi is not prevented, and the material remains degradable by fungi. Ringman et al. showed that fungi can degrade thermally modified wood to substantial

Received: August 8, 2025
Revised: September 20, 2025
Accepted: September 22, 2025
Published: October 1, 2025

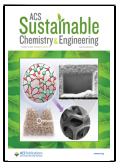

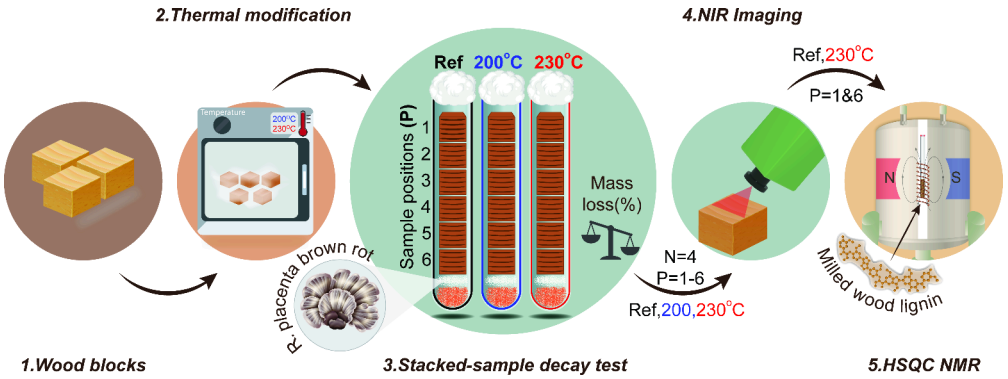

Figure 1. Experimental workflow for wood decay analysis: (1) Wood blocks. (2) Thermal modification at 200 and 230 °C. (3) Stacked-sample decay test using *R. placenta* (sample positions labeled 1−6) followed by mass loss measurement for all samples (N = 7, positions 1−6, all sample types). (4) NIR imaging of a subset of samples (N = 4, positions 1−6, all sample types). (5) Lignin isolation from pooled samples (positions 1 and 6, reference and 230 °C samples) followed by HSQC NMR.

mass loss over time,[20] but otherwise, the actual fungal degradation of thermally modified wood has received little attention. Recent research into other decay resistant wood materials has revealed that wood decaying fungi can degrade the chemical constituents responsible for the increased decay resistance in some materials but not others,[21−25] highlighting the need for research on thermally modified wood. To fill this need, we recently studied the degradation of thermally modified wood by brown rot fungi.[26] We found that the early stages of decay were associated with a rapid increase in hygroscopicity, suggesting that fungi can degrade the chemical alterations responsible for decay resistance in thermally modified wood as well.

Here, we continue our investigation of thermally modified wood degradation with an in-depth chemical analysis of the previously studied samples using advanced analytical methods. We focus our analysis on wood degraded by *Rhodonia placenta*, a fungus that proved to be particularly effective in degrading thermally modified wood.[26] We collected NIR spectral data from a larger set of samples and analyzed the data by ANOVA simultaneous component analysis (ASCA) and partial least-squares regression (PLSR) to gain detailed insight into the degradation of the wood cell wall polymers. We also isolated milled wood lignin from the degraded samples for detailed characterization of lignin degradation by 2D $^{1}H-^{13}C$ heteronuclear single quantum coherence nuclear magnetic resonance (HSQC NMR) spectroscopy. The objective of our study was to uncover the chemical changes associated with *R. placenta* degradation of thermally modified and unmodified wood and understand the characteristic features of thermally modified wood degradation. The results increase our understanding of wood degradation mechanisms and provide insights for optimizing sustainable wood protection technologies.

MATERIALS AND METHODS

Sample Preparation. The wood samples used in this experiment were the same as those used in our previous study focusing on hygroscopicity changes.[26] The samples were prepared from Scots pine sapwood and had dimensions of 8 × 8 × 12 mm^3 (T × R × L). The samples were free of knots, growth anomalies, cracks, and other defects to avoid variations in the initial structure and chemical composition. The samples were first dried at 105 °C for 24 h to determine their initial dry mass and then thermally modified in an oven under superheated steam at atmospheric pressure. One set of samples (N = 42) was modified at 200 °C and one at 230 °C; one was left unmodified. The heating program was as follows: (1) 30 min at 105 °C in the absence of steam, (2) introduction of steam and a stepwise increase in temperature (15 °C every 15 min) until the final modification temperature, and (3) 3 h at the final modification temperature. After modification, the samples and the unmodified references were impregnated with deionized water and leached for 2 weeks with frequent water changes (every 1−3 days). The leached samples were dried at room temperature for 24 h and then at 105 °C for another 24 h to determine their modified dry mass. The mass losses due to modification at 200 and 230 °C were 5.9 ± 0.5% and 12.2 ± 0.5%, respectively.

Decay Test. Before the decay test, all samples were sterilized by ionizing radiation (25−50 kGy dose) and conditioned at 85% RH over a saturated solution of KCl for 8 weeks. The decay test was a stacked-sample test as reported in ref 26. The test was conducted in test tubes, which contained 4 mL of 2% malt extract agar inoculated with a plug of mycelium from *R. placenta* (strain BAM 113) stock cultures maintained on 2% malt extract agar plates. Each inoculated tube received six wood samples stacked on top of each other (sample positions 1−6; see Figure 1). Seven replicate tubes were prepared per sample type. A piece of plastic netting was placed between the mycelial plug and the bottommost sample in each tube to prevent moisture absorption from the agar. The tubes were plugged with cotton wool and incubated at 85% RH (saturated solution of KCl) and room temperature for 33 weeks. After decay, the samples were brushed to remove surface mycelium and dried at room temperature for 24 h and then at 105 °C for another 24 h to determine their decayed dry mass and mass loss due to decay. The experimental workflow and the subsequent analyses are summarized in Figure 1.

NIR Spectroscopy and Data Analysis. *Spectral Acquisition and Preprocessing.* NIR imaging was performed on all sample types. Four out of seven replicate tubes per sample type were selected for imaging. Tubes with mass losses closest to the average for that sample type were selected. Before imaging, the radial sample surfaces were cut with a microtome to reduce surface roughness and eliminate height differences. The radial surface was selected over the cross-sectional surface to reduce damage to the highly fragile decayed samples. The microtome-smoothed samples were stored in sealed tubes with silica gel until imaging to prevent moisture absorption. NIR spectra were acquired in reflectance mode from the radial sample surfaces as before[27,28] using a Specim SWIR (Specim, Spectral Imaging, Ltd.) short wavelength infrared hyperspectral camera equipped with an OLES macro lens with a field of view of 10 mm, two halogen lamps to generate polychromatic light, and a HgCdTe detector array with a grating prism monochromator to gather the reflected wavelengths from the exposed sample surface. The samples to be imaged were placed on a vertical translation stage under the camera, and the height of the stage was adjusted to match each sample surface with the focal plane of the camera. Images were recorded in line scanning mode, with each scan recording 384 pixels and 288 spectral variables over a

https://doi.org/10.1021/acssuschemeng.5c08352
ACS Sustainable Chem. Eng. 2025, 13, 17050−17060

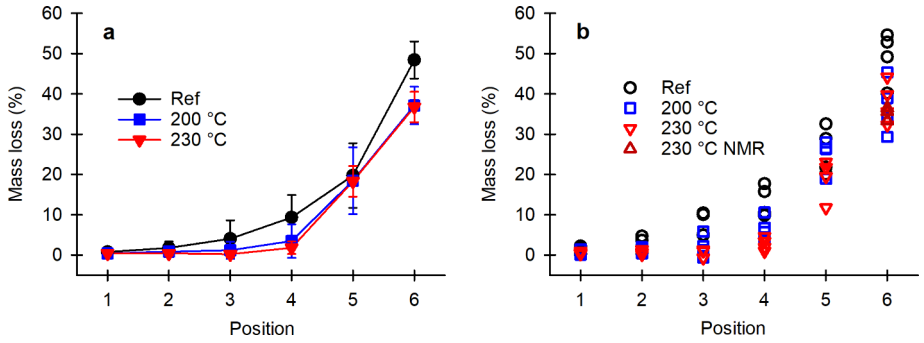

Figure 2. Average (N = 7) decay mass losses of reference (ref) and thermally modified (200 and 230 °C) samples (a) and individual decay mass losses of samples selected for NIR and NMR analyses (b) as a function of sample position in the decay test. The NMR analyses were conducted on position 1 and position 6 of the samples used for NIR (except for the position 6 thermally modified (230 °C) samples, which used the replicate samples not used for NIR). The error bars in panel a are ± standard deviation

spectral range of 930−2550 nm at a spectral resolution of 12 nm (full width at half-maximum). A calibration reflectance target was scanned along with the samples, resulting in overall image dimensions of 1244 × 384 pixels.

Raw images were transformed from digitalized signal (2^{16} units) to reflectance using the spectral reflectance target and dark current intensities.[29] The corrected images were processed using principal component analysis[30] with background pixels removed through score-based thresholding, followed by median filtering with a 3 × 3 pixel window to eliminate saturated pixels. For each sample image, the center was located, and a fixed-size rectangular region of interest (ROI) was extracted while excluding edge artifacts. Images were then converted to absorbance using $A = \log_{10}(1/r)$, where A represents the estimated absorbance and r is the unitless reflectance value.[31] An average spectrum was calculated for each sample, and the resulting average absorbance spectra were preprocessed using Savitzky−Golay filtering[32] by fitting a second-order second-derivative polynomial on a moving window of 15 variables. Finally, the filtered spectra were mean-centered by subtracting the average spectrum from the data set.

Multivariate Data Analyses. First, the spectral changes generated by the controlled experimental conditions were isolated with ANOVA simultaneous component analysis (ASCA).[33] The effects of modification, position, and biological replicate and their two-factor interactions were determined with the ASCA decomposition described in more detail in our previous work.[27,34] The final ASCA scores for an effect were determined by summing the decomposed ASCA scores with the residual scores, which were determined by projecting the model residuals onto the ASCA loadings.[35] Finally, the statistical significance of the isolated effects was estimated by comparing the sum-of-squares of an effect matrix to a background distribution of random sum-of-squares determined by permutations. The permutations were done by randomly permuting the row indices of the preprocessed and mean-centered spectra 1000 times[36] and the effect matrices and their sum-of-squares were then determined as described above. The computations were done using in-house Matlab (The MathWorks Inc.) scripts, including functions from the PLS toolbox (eigenvector Research Inc.). The two-factor interactions were found to be statistically insignificant and, therefore, were left out of the final ASCA model.

Second, the preprocessed spectra were separated into three groups according to sample type (reference, 200 °C, and 230 °C). For each group, separate partial least-squares regression (PLSR) models were developed using the SIMPLS algorithm[37] to correlate the spectral data with the measured mass losses. The number of latent variables was selected for each treatment model based on the root-mean-square error of calibration (RMSEC) and cross-validation (RMSECV). Although n = 2 provided the lowest errors for the reference model, we used n = 2 for all models to allow comparison between the sample groups. Cross-validation was performed by dividing the data set into five subgroups, systematically excluding each subgroup from calibration for validation purposes. The regression coefficients from all three models were compared. The spectral regions strongly influencing mass loss prediction were determined by calculating the Variable Importance in Projection (VIP) scores.[38] Spectral regions yielding VIP scores >1 were identified as significant contributors to the predictive model, indicating areas of interest related to chemical changes caused by the treatments. Data preprocessing and PLSR were performed using in-house MATLAB scripts (MATLAB 2023a, The MathWorks Inc.) and the PLS Toolbox version 9.3 (eigenvector Research Inc.).

Lignin Isolation and HSQC NMR. Lignin isolation and NMR analyses were performed on the reference and 230 °C thermally modified samples from decay test sample positions 1 and 6 as well as on unmodified Scots pine sapwood not exposed to fungi to provide a control. The same four replicate samples were used as for NIR imaging, except for the position 6 thermally modified samples (the samples used for NIR were lost during lignin isolation, so the lignin was isolated from the remaining three replicate samples). Pooled replicate samples were first ground in a knife mill (IKA A10) and then Soxhlet extracted for 5 h using toluene:ethanol (2:1).[39] The extracted residues were ball milled in a Fritsch Planetary 6 Ball Mill using an 80 mL milling cup with 20 ZrO_2 balls with 10 mm diameter. The total milling time was 24 h, with sequential 15 min of milling at 450 rpm followed by a 15 min pause to cool down. After milling, the samples were extracted twice in 1,4-dioxane at 30 °C in an ultrasound bath,[40] after which the combined filtrations were evaporated in a rotary evaporator to yield milled wood lignin. The isolated yields varied from 9.7 mg for the unmodified and unexposed control to 44.8 mg for most decayed wood sample.

The lignin samples were dissolved without further purification in 0.5 mL of acetone-d_6 and analyzed using $^{1}H-^{13}C$ HSQC correlation NMR experiments. A Bruker AV NEO 600 MHz spectrometer equipped with a 5 mm TCI cryoprobe was used for measurements. The HSQC spectra were recorded using the Bruker standard pulse sequence (hsqcetgpsisp.2), with a spectral width of 11 ppm in the F2 (^{1}H) dimension and 212 ppm in the F1 (^{13}C) dimension. For each spectrum, 52 scans were measured by using a 1.44 s relaxation delay and 16 dummy scans. The acetone solvent signal at 2.05/29.92 ppm was used for referencing the spectra, and the cross signals were assigned according to literature.[41] All spectra were processed by using Bruker TopSpin 4.4.1 software with standard parameters. Semi-quantitative spectral analysis of the HSQC spectra was performed, and the HSQC cross signals were volume integrated against 100 aromatic units.[42,43] The values are presented based on integrals relative to $G_2 + G_2ox' + H_{3,5}/2 = 100$.

RESULTS AND DISCUSSION

Decay Progression. The thermally modified and unmodified reference samples were exposed to *R. placenta* in a stacked-sample decay test. The average mass losses of the samples are given in Figure 2a as a function of mass loss, while

https://doi.org/10.1021/acssuschemeng.5c08352
ACS Sustainable Chem. Eng. 2025, 13, 17050−17060

the individual mass losses of the samples selected for NIR and NMR are given in Figure 2b. As previously reported,[26] *R. placenta* caused a nonlinear increase in mass loss with sample position in all three sample types. In the unmodified references, mass loss increased from 1% at position 1 to 48% at position 6. The samples thermally modified at 200 and 230 °C showed virtually identical patterns of mass loss. Mass loss remained low until position 4, after which it rapidly increased to 37% at position 6 in both modified sample types. The results confirm that *R. placenta* is an effective degrader of thermally modified wood, as previously demonstrated in several experiments.[44−46] The mass losses of the samples selected for NIR and NMR were representative of the average mass loss of each sample type (Figure 2b).

NIR Characterization and Multivariate Analysis. *ANOVA Simultaneous Component Analysis (ASCA).* To gain more insight into how *R. placenta* degrades thermally modified wood, the previous NIR spectroscopic analysis of the samples[26] was expanded. NIR images were collected from a larger set of samples, after which average spectra were extracted from the images, converted to second derivative, and analyzed first by ASCA to identify the key spectral features associated with thermal modification and decay. The explained variation and statistical significance of the main effects (modification, position in the decay test, replicate) are given in Table 1. The modification and position were statistically

Table 1. Explained Variation and Significance of the Main Effects from ASCA

Effects	Variation (%)	*p*-value
Modification	11.7	0.009
Position	66.3	0.000
Replicate	1.1	0.950
Residual	20.9	
Sum	99.999	

significant ($p < 0.05$), explaining 12% and 66% of the data variation, respectively, while the replicate effect was statistically insignificant. The interaction effects were statistically insignificant and excluded from the model.

The ASCA loadings and score plots of the modification and position effects are presented in Figure 3. ASCA was performed on second derivative spectra, which means that positive loadings and scores correspond to a decrease in band intensity, while negative loadings and scores correspond to an increase in band intensity. The first component loading of the modification effect had positive bands at 1426, 1926, and 2047 nm and negative bands at 1315, 1393, 1881, and 1992 nm. The positive bands at 1426 and 1926 nm were assigned to amorphous polysaccharides[47,48] and hemicellulose,[48] respectively. The band at 2047 nm could not be assigned. The negative bands at 1393 and 1881 nm were tentatively assigned to lignin OH[48] and C═O[49] groups, respectively. The negative bands at 1315 and 1992 nm could not be assigned. However, a band has been previously detected at approximately 1990 nm in brown rotted wood together with other lignin-derived bands,[27] which means that the 1992 nm band is likely to be lignin-derived. The second component loading in turn had positive bands at 1364 and 2097 nm assigned to cellulose.[48,50] Negative bands were found at 1315 and 2258 nm. The 1315 nm band remains unassigned, while the 2258 nm band, which is known to occur on lignin,[27,50] was tentatively assigned to the C−H + C═O combination of aldehyde/acetyl groups.[48,51,52] Due to the use of second derivative spectra, the first component therefore gives positive scores to samples with strong spectral contributions from lignin (tentative OH and C═O and unknown functionality) relative to amorphous polysaccharides, while the second component gives positive scores to samples with strong spectral contributions from lignin (tentative C═O) relative to cellulose.

The modification effect separated the sample types when the scores of the first ASCA component were plotted against those of the second ASCA component. The samples modified at 230 °C, in particular, were separated from the reference and 200 °C samples. The scores of the first ASCA component increased with modification, indicating an increase in lignin OH, C═O, and unknown functionality and a decrease in amorphous polysaccharide content with modification. The degradation of amorphous polysaccharides is the most notable chemical change caused by thermal modification [e.g., 4], and while conflicting reports exist on the chemical changes to lignin, several investigations have found an increase in the concentration of phenolic OH[6−8,49,53] as well as C═O groups.[53,54] The second ASCA component gave slightly lower scores for the samples modified at 200 °C than the other samples, indicating that they had a higher cellulose content relative to lignin C═O functionality than the reference samples. Thermal modification has been shown to increase cellulose content[5] and crystallinity[55] at lower modification intensities. Otherwise, the second component scores correlated with the first component scores.

The first component loading of the position effect had positive bands at 1920, 2086, and 2479 nm and negative bands at 1665, 1876, 2014, 2235, and 2412 nm. The positive bands were assigned to carbohydrates: 1920 nm to hemicellulose, 2086 nm to cellulose, and 2479 nm tentatively also to cellulose.[48,50] The negative bands were assigned to lignin: 1665 nm to the aromatic ring,[48] 1876 and 2235 nm tentatively to C═O, and 2412 nm to unknown functionality.[27,50] The 2014 nm band could not be assigned, but a similar band was detected in wood degraded by *R. placenta* together with other lignin-derived bands,[27] which suggests that it is likely to be lignin-derived. The second component loading had positive bands at 1443, 1870, 2075, and 2490 nm and negative bands at 1398, 1920, and 2235 nm. The band at 1443 nm was tentatively assigned to lignin phenolic OH,[48] while the other positive bands were assigned to lignin C═O (1870 nm) and cellulose (2075 and 2490 nm) as described above. The negative band at 1398 nm was again tentatively assigned to lignin OH groups, while the bands at 1920 and 2235 nm were assigned to hemicellulose and lignin C═O, respectively. Due to the use of second derivative spectra, the first component therefore gives positive scores to samples with strong spectral contributions from lignin (aromatic, C═O, and unknown functionality) relative to carbohydrates, while the second component gives positive scores to samples with strong spectral contributions from hemicellulose and lignin (OH and C═O) relative to cellulose and lignin (phenolic OH and C═O).

The scores of the first and second ASCA components of the position effect separated the samples according to position in the decay test tubes. The first component scores increased gradually from position 3 onward, indicating a decrease in carbohydrate content and an increase in residual lignin content with increasing decay. Lignin showed an increase particularly

https://doi.org/10.1021/acssuschemeng.5c08352
ACS Sustainable Chem. Eng. 2025, 13, 17050−17060

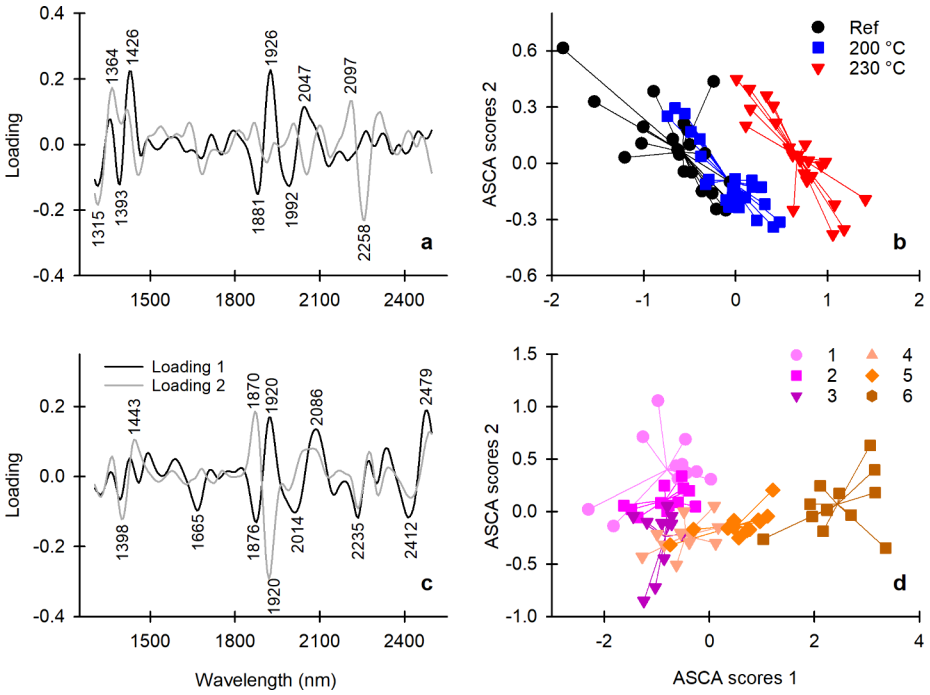

Figure 3. First and second ASCA component loadings (a, c) and scores (b, d) of the modification effect (a, b) and the position effect (c, d). ASCA was performed on second derivative spectra, which means that positive loadings and scores correspond with a decrease in band intensity, while negative loadings and scores correspond with an increase in band intensity.

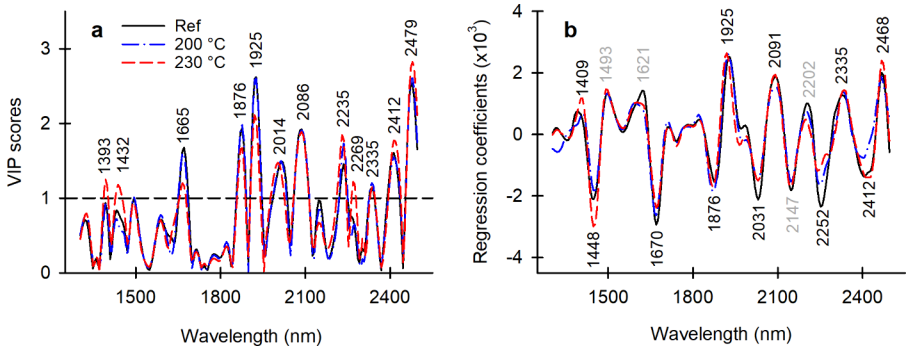

Figure 4. VIP scores (a) and regression coefficients (b) of the PLSR models predicting mass loss in the reference (ref) and thermally modified (200 and 230 °C) samples. Variables with VIP scores >1 are considered significant. Bands in panel b with VIP scores >1 are labeled in black and bands with VIP scores <1 are labeled in gray. PLSR was performed on second derivative spectra, which means that positive regression coefficients correspond with a decrease in band intensity, while negative coefficients correspond with an increase in band intensity.

in aromatic, C═O, and unknown functionality. The second component scores, in turn, decreased from position 1 until position 3 and then increased again slightly from position 4 to position 6. The pattern indicates an increase in the levels of cellulose and lignin (phenolic OH and C═O) relative to those of hemicellulose and lignin (OH and C═O) in incipient decay, followed by the reverse trend in more advanced decay. The overall decrease in carbohydrate content with an initial increase in cellulose relative to hemicellulose is consistent with the known brown rot degradative mechanism. Brown rot fungi degrade the wood cell wall carbohydrates, with preferential degradation of hemicelluloses in early decay and simultaneous degradation of cellulose and remaining hemicelluloses in later decay.[56,57]

The chemical changes to lignin also agree with previous knowledge, although some new patterns also emerged. Brown rot fungi cause lignin demethylation, side chain oxidation, and side chain cleavage, which in turn cause an increase in phenolic OH, an increase in side chain C═O with a decrease in side chain OH, and the production of new chain ends with hydroxyl, carbonyl, or carboxyl groups.[58−62] Direct aromatic hydroxylation is considered unlikely.[59,60] The continuing increase in lignin aromatic and C═O functionality identified by ASCA is consistent with an overall increase in lignin content and agrees with the previously documented oxidative changes. However, the ASCA results suggested that lignin undergoes changes in the OH and C═O group distribution over the course of decay. The initial increases in phenolic OH and C═O are most likely caused by demethylation and side chain oxidation, respectively,[58,59,61] although aromatic hydroxylation could also cause an increase in phenolic OH. The decrease in phenolic OH and C═O relative to other OH and C═O in more advanced decay stages most likely reflects a decrease in the rate of phenolic OH and C═O generation relative to other OH and C═O. New nonphenolic OH groups may be generated by side chain cleavage,[60,62,63] while the continued

https://doi.org/10.1021/acssuschemeng.5c08352
ACS Sustainable Chem. Eng. 2025, 13, 17050−17060

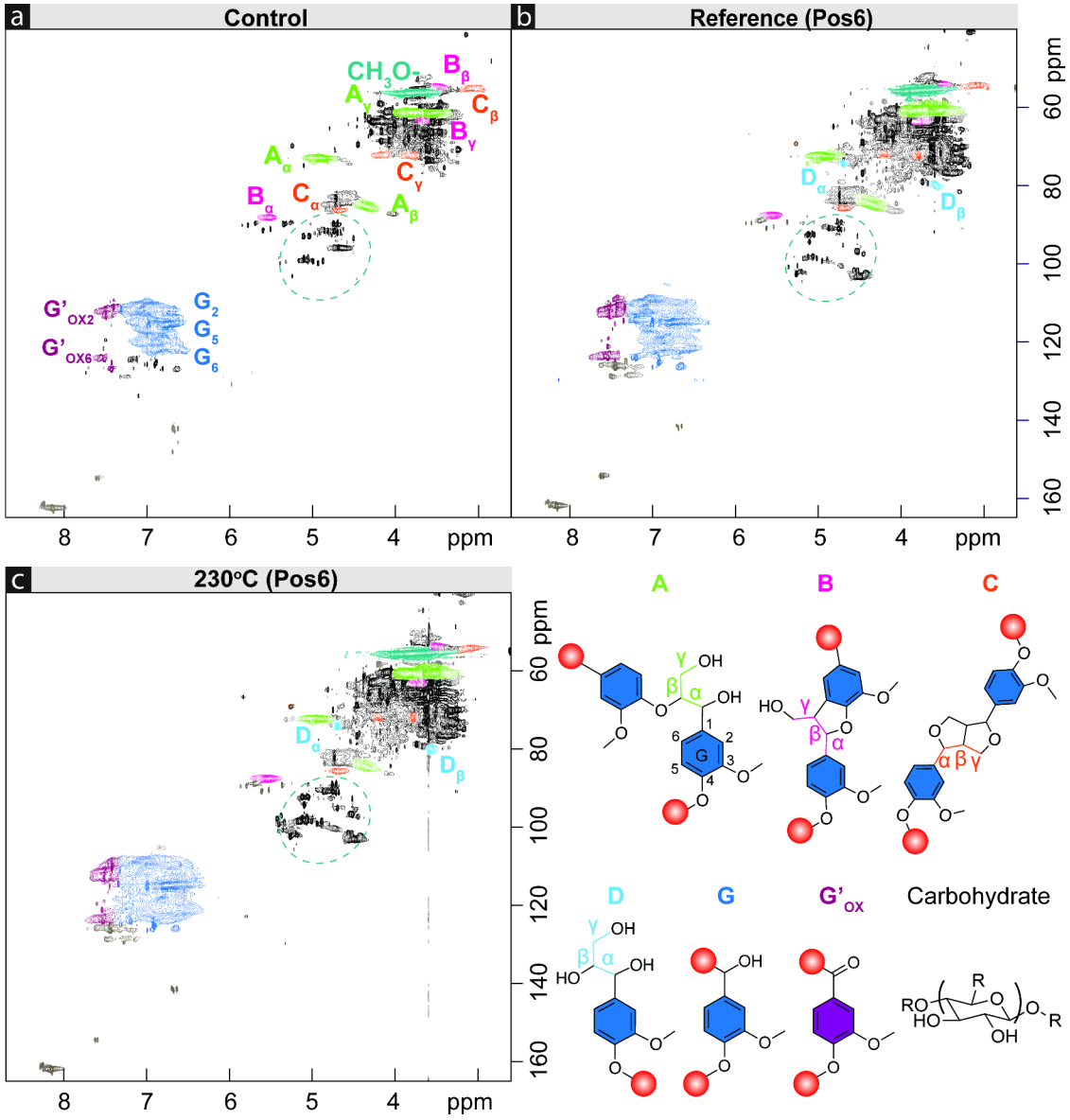

Figure 5. HSQC NMR spectra of milled wood lignin from unmodified and unexposed control wood (a), most decayed (position 6) reference samples (b), and most decayed (position 6) thermally modified (230 °C) samples (c). Structures A–D represent side chain structures, G is the aromatic guaiacyl unit, and G′$_{ox}$ is an oxidized G-unit with an aldehyde, ketone, or carboxylic structure. Carbohydrate represents various solubilized carbohydrates in the lignin samples, emphasized with a dashed green circle.

oxidation of OH may alter the distribution and type of C═O containing groups.

Partial Least-Squares Regression (PLSR). After identifying the key spectral changes associated with modification and decay using ASCA, average image spectra were used to estimate mass loss with partial least-squares regression. Separate regression models were built for the three different sample types to explore the degradative differences between them. The VIP scores and regression coefficients of the models are given Figure 4, while the root-mean-square errors and plots of observed vs predicted mass loss are given in Supplementary Figure S1. PLSR was performed on second derivative spectra, which means that positive regression coefficients correspond to a decrease in band intensity, while negative coefficients correspond to an increase in band intensity. The VIP scores (Figure 4a) identified ten bands as important in all three sample types: 1665 nm (lignin aromatic), 1878 nm (lignin C═O), 1925 nm (hemicellulose), 2014 nm (unidentified, likely lignin-derived), 2086 nm (cellulose), 2235 nm (lignin C═O), 2335 nm (cellulose or hemicellulose[48]), 2412 nm (lignin unknown), and 2479 nm (cellulose). The regression vectors (Figure 4b) showed positive regression coefficients for the carbohydrate-derived bands and negative coefficients for the lignin-derived bands, consistent with preferential carbohydrate degradation and in agreement with the position-related changes identified by the ASCA.

Despite the similarities, the VIP scores and regression vectors also identified some differences among the sample types. In the samples modified at 230 °C, VIP indicated three additional important bands at 1393, 1437, and 2269 nm. The 1393 and 1437 nm bands were tentatively assigned to lignin OH groups, while the 2269 nm band was assigned to lignin C═O. The regression vectors showed that the 1409 nm band (1393 nm in VIP) had a positive regression coefficient in all

https://doi.org/10.1021/acssuschemeng.5c08352
ACS Sustainable Chem. Eng. 2025, 13, 17050−17060

Table 2. Relative Integrated Peak Areas from Semiquantitative HSQC NMR Spectra of Milled Wood Lignin Exposed to *R. placenta*[a]

Structure	Control	Reference		Modified (230 °C)	
		Position 1	Position 6	Position 1	Position 6
G	78.2	74.6	79.6	74.3	77.5
G'_{ox}	20.8	23.8	19.4	24.8	21.7
Methoxyls	77.7	69.7	67.9	69.2	71.2
β-O-4 (A)	25.5	23.3	20.5	9.3	9.8
β-5 (B)	8	6.9	7.4	8.6	7.8
β-β (C)	9.1	8.1	5.5	3.2	3.6
Phenyl glycerol (D)	3.7	6	5.5	4.1	4.3
Carbohydrates	68.6	86	49	81	67
Aldehydes	11.3	14.1	13.9	11.5	10.5

[a]Values are normalized to 100 aromatic units. Samples include an unmodified, unexposed control; reference samples with least (Position 1) and most (Position 6) decay; and thermally modified (230 °C) samples with least (Position 1) and most (Position 6) decay.

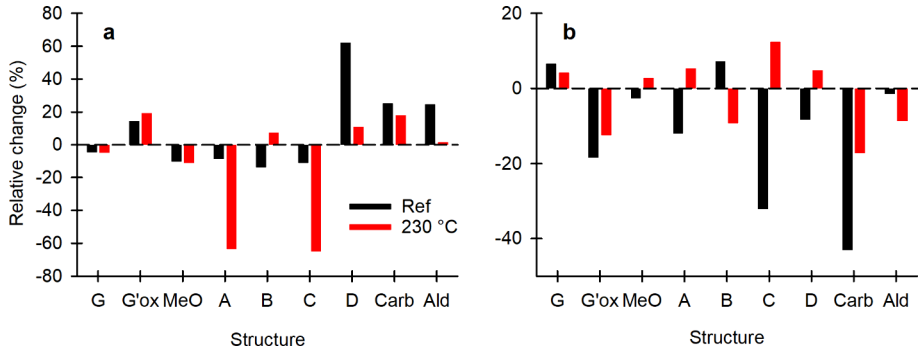

Figure 6. Changes in relative integrated peak areas calculated from semiquantitative HSQC NMR spectra in the reference (ref) and thermally modified (230 °C) samples: position 1 relative to the unmodified and unexposed control (a) and position 6 relative to position 1 (b). MeO, methoxyls; carb, carbohydrates; ald, aldehydes.

sample types, while the 1448 nm band (1437 nm in VIP) had a strong negative coefficient. Due to the use of second derivative spectra, the 1409 nm band therefore decreased with mass loss, while the 1448 nm band increased with mass loss. The 2269 nm band did not appear as a separate band on the regression vectors but as a shoulder on the 2252 nm band. The ASCA results (Figure 3c,d) indicated that early decay was associated with an increase in phenolic OH relative to other OH and late decay with the reverse. However, the regression vectors revealed that the 1448 nm phenolic OH band showed an overall increase with mass loss, and the 1409 nm OH band had an overall decrease. However, these changes were significant only in thermally modified wood, which suggests that *R. placenta* degradation has different effects on lignin in thermally modified wood and unmodified wood. Thermally modified wood also showed less negative regression coefficients at 1670, 2031, and 2252 nm than unmodified wood, indicating further differences between the sample types in lignin degradation.

Lignin Characterization by HSQC NMR. Given the significance of lignin in understanding the degradation of thermally modified wood, the chemical changes to lignin were investigated further using HSQC NMR. Milled wood lignin was isolated from the least decayed (position 1) and most decayed (position 6) reference and thermally modified (230 °C) samples and from unmodified Scots pine sapwood not exposed to fungi as a control. The HSQC spectra of the control and position 6 lignins are shown in Figure 5, while spectra of the position 1 lignins can be found in Supplementary Figure S2. All spectra showed typical softwood lignin features such as guaiacyl aromatic units (G) and the most prevalent interunit linkages, such as aryl ether β−O−4 (A), phenylcoumaran β−5 (B), and resinol β−β (C). Some differences could, however, be seen between the spectra. Most importantly, the decayed reference and modified samples showed decreased signals from G-units, methoxyl groups, and interunit linkages (A, B, C) and increased signals from different oxidized structures. In the aromatic region, the decayed samples showed an increase at δ_H/δ_C 7.43/112 ppm and 7.52/124 ppm, which correspond to oxidized guaiacyl structures (correlation signals in aromatic ring positions 2 and 6, respectively) originating from the formation of aldehyde, ketone and carboxyl groups at the benzylic position (G'_{ox}). The spectra of decayed samples also suggested some unspecific oxidation of G-units to catechol, quinone, and enol ether structures that mainly appeared as overlapping CH correlation signals and an overall broadening of the aromatic area. In the oxygenated aliphatic area, new signals appeared at δ_H/δ_C 4.62/74.7 ppm and 3.57/79.9 ppm, which correspond to phenylglycerol structures (D). The position 1 decayed samples (see Supplementary Figure S2) also showed an increase in the carbohydrate anomeric carbon C1 area at δ_H/δ_C 4.2−5.5/90−106 ppm and other carbohydrate-originating signals at 3.2−4.3/62−78 ppm, which indicated that carbohydrate degradation by *R. placenta* resulted in increased carbohydrate solubilization in the isolated lignin fractions.

For semiquantitative analysis, the relative integrated peak areas of the different structures were calculated to compare their abundances in the samples. Table 2 gives the calculated peak areas for all samples, while Figure 6 shows the relative changes in peak area caused by decay by comparing the

https://doi.org/10.1021/acssuschemeng.5c08352
ACS Sustainable Chem. Eng. 2025, 13, 17050−17060

position 1 samples to the control (Figure 6a) and the position 6 samples to position 1 (Figure 6b). Relative to the control, the position 1 references showed an increase in oxidized structures (G'_{ox} and D) and a decrease in unoxidized G-units, methoxyls, and interunit linkages (A, B, and C). There was also an increase in aldehydes (δ_H/δ_C 9.76/191.8 and 9.55/194.8 ppm) and unspecific oxidation and a large increase in solubilized carbohydrates based on the increased anomeric signals. The position 6 samples in turn showed a decrease in the oxidized structures G'_{ox} and D relative to position 1 and a notable increase in the strongly oxidized unspecific aromatic structures. The samples also showed a continued decrease in methoxyls and A and C interunit linkages, while aldehydes remained at an elevated level. The content of solubilized carbohydrates decreased dramatically.

The structural changes seen in the reference samples suggest that *R. placenta* degradation of unmodified pine caused G-unit oxidation, demethylation, and interunit linkage degradation (side chain alkyl-aryl cleavage) in lignin, in agreement with previous studies.[58−63] Interunit linkage degradation appears to involve both β−O−4́ linkages (A) and β−β linkages (C), in agreement with Martínez et al.[63] and in contrast to the A-only degradation found by Yelle et al.[62] and Rese et al.[60] The initial decay stages were characterized by side chain oxidation, demethylation, and interunit linkage degradation, as evidenced by the increase in G'_{ox}, D, and aldehydes and the decrease in methoxyls and interunit linkages. The advanced decay stages were in turn characterized by continued interunit linkage degradation and advancing G-unit oxidation, which can be seen as a decrease in the oxidized structures G'_{ox} and D and a strong increase in highly oxidized structures. The increase in signals in the δ_H/δ_C 6.3−7.3/108−125 ppm range suggests that *R. placenta* degradation caused recondensation, hydroxylation, and quinone formation, but the overlapping signals prevent more detailed structural assignments. Condensed structures have been detected in brown rotted lignin,[60] while direct aromatic hydroxylation by hydroxyl radicals is considered unlikely, at least in some studies.[59,60] The structural changes revealed by HSQC agree with the chemical changes highlighted by ASCA (Figure 3c,d) and PLSR (Figure 4). Both ASCA and PLSR indicated an increase in lignin C═O with decay, which is consistent with side chain oxidation as well as potential quinone formation. ASCA also showed that wood degraded by *R. placenta* underwent changes in OH and C═O distribution over the course of decay, in agreement with the increase in G'_{ox} and D in early decay and the subsequent decrease in G'_{ox} and D and the increase in unspecific changes in later decay.

Relative to the unmodified control, the position 1 thermally modified samples showed a strong increase in unspecific oxidation and a strong decrease in the number of A (β-O-4) and C (β-β) interunit linkages. G'_{ox}, D, and carbohydrates increased as well, while methoxyls decreased. No modified control samples were analyzed, which means that the effects of modification and decay cannot be separated in the position 1 thermally modified samples. However, most of the differences between the control and position 1 modified samples were likely due to the modification. Compared to the references, the thermally modified samples showed much more prominent unspecific oxidation, more prominent changes in A and C, and less prominent or no changes in side chain-degraded products D, aldehydes, and carbohydrates. The strong increase in highly oxidized and recondensed G-units and the strong decrease in interunit linkages (A and C) due to modification are consistent with previous findings[7,8,53,64] and the ASCA results (Figure 3a,b), which revealed an increase in lignin OH and C═O in the thermally modified samples. The position 6 samples revealed the effects of decay in the thermally modified wood. Like the position 6 references, the position 6 thermally modified samples exhibited a decrease in G'_{ox} relative to position 1 and a strong increase in unspecific changes. However, the increase in unspecific changes from position 1 to 6 was less pronounced in the modified samples than in the references. The modified samples also showed a slight increase in A, C, and methoxyls, a small decrease in B and aldehydes, and no change in D. These changes are in contrast to the changes seen in the references, which included a decrease in A, C, D, and methoxyls, an increase in B, and no changes in aldehydes.

The structural changes seen in the thermally modified samples suggest that *R. placenta* degradation caused similar yet different chemical changes in modified wood than unmodified wood, in agreement with the VIP and PLSR (Figure 4) results. The effects of incipient decay could not be reliably established due to the lack of modified controls, but the position 6 samples revealed details about the changes associated with advanced decay. Relative to position 1, the position 6 modified samples showed progressing G-unit oxidation as evidenced by the decrease in G'_{ox} and the increase in unspecific oxidized structures, similar to the references. However, the modified samples showed a smaller increase in unspecific oxidation than the references, possibly due to the high level of unspecific oxidation caused by the modification itself. The reduced magnitude of unspecific oxidation in the modified samples may explain the VIP and PLSR results (Figure 4), which indicated that the small decrease in one OH population and the strong increase in another (likely phenolic) OH population were significant only in the samples modified at 230 °C. The reduced oxidation of G'_{ox} in modified wood compared to that in unmodified wood may explain why modified wood showed a stronger increase in phenolic OH with decay. However, the unspecific nature of the various oxidized structures complicated interpretation. Relative to position 1, the position 6 modified samples also showed an increase in several unoxidized structures (methoxyls, A, and C) and a decrease in aldehydes. These changes indicate that advanced decay caused further degradation of already oxidized structures, increasing the relative abundance of the unoxidized structures. The progressing degradation of oxidized structures in advanced decay is similar to the changes seen in unmodified wood. However, it is clear that the exact degradative pathways were different.

CONCLUSIONS

R. placenta caused carbohydrate degradation and lignin modification in thermally modified and unmodified wood, as expected for brown rot. In agreement with previous knowledge, NIR spectroscopy in combination with ASCA showed that carbohydrate degradation was characterized by preferential hemicellulose degradation in early decay and by increasing cellulose degradation in advanced decay. The oxidative changes to lignin revealed by ASCA, PLSR, and HSQC NMR were also in agreement with previous knowledge and included G-unit oxidation, demethylation, and interunit linkage degradation along with an overall increase in aromatic and C═O functionality. However, the analyses showed for the

https://doi.org/10.1021/acssuschemeng.5c08352
ACS Sustainable Chem. Eng. 2025, 13, 17050−17060

first time that the oxidative changes in lignin evolved over the course of decay. ASCA showed that there were changes to lignin OH and C=O distributions over the course of decay, while HSQC NMR analysis of the reference and 230 °C modified samples provided mechanistic insights into these transformations. Applied to brown rotted samples in incipient decay for the first time, HSQC showed that early decay involved side chain oxidation, demethylation, and interunit linkage degradation, while advanced stages were characterized by progressing degradation of already oxidized structures. Both NIR and NMR indicated that the degradation of thermally modified wood proceeded by a mechanism similar to that of unmodified wood. However, compared to unmodified wood, the samples modified at 230 °C showed more prominent changes in lignin OH groups and differences in the degradation of already-oxidized structures. These findings shed new light on *R. placenta* wood degradation mechanisms, which support the continued development of wood protection methods for sustainable construction materials.

■ ASSOCIATED CONTENT

Data Availability Statement

The NIR hyperspectral imaging dataset generated in this study is available in the Zenodo repository at doi.org/10.5281/zenodo.15828807. The corresponding NMR dataset is available from the authors upon reasonable request.

Supporting Information

The Supporting Information is available free of charge at https://pubs.acs.org/doi/10.1021/acssuschemeng.5c08352.

PLSR model validation data including root-mean-square error plots for calibration and cross-validation, observed vs predicted mass loss plots for reference and thermally modified samples, and two-dimensional HSQC NMR spectra of milled wood lignin from control and decayed samples at different decay stages (PDF)

■ AUTHOR INFORMATION

Corresponding Authors

Tiina Belt − *Natural Resources Institute Finland, Production Systems, 00790 Helsinki, Finland*; Email: tiinabelt@gmail.com

Muhammad Awais − *Department of Bioproducts and Biosystems, Aalto University, FI-02150 Espoo, Finland; Norwegian University of Life Sciences, Faculty of Science and Technology, Ås 1433, Norway*; orcid.org/0000-0002-2265-6612; Email: muhammad.awais@aalto.fi

Authors

Paula Nousiainen − *Department of Bioproducts and Biosystems, Aalto University, FI-02150 Espoo, Finland*; orcid.org/0000-0002-7089-1158

Lauri Rautkari − *Department of Bioproducts and Biosystems, Aalto University, FI-02150 Espoo, Finland*; orcid.org/0000-0002-1207-220X

Mikko Mäkelä − *VTT Technical Research Centre of Finland Ltd, VTT, FI-02044 Espoo, Finland*; orcid.org/0000-0001-6174-6330

Complete contact information is available at: https://pubs.acs.org/10.1021/acssuschemeng.5c08352

Author Contributions

T.B.: conceptualization; funding acquisition; investigation; methodology; resources; visualization; writing—original draft; writing—review and editing. M.A.: formal analysis; investigation; software; visualization; writing—review and editing. P.N.: methodology; visualization; writing—review and editing. L.R.: supervision; writing—review and editing. M.M.: formal analysis; software; writing—review and editing.

Notes

The authors declare no competing financial interest.

■ ACKNOWLEDGMENTS

This work was supported by the Research Council of Finland (grant numbers 330087, 349198, and 341701), the Research Council of Finland's FinnCERES (Competence Center for Materials Bioeconomy) flagship programme (grant number 345553), the Finnish Cultural Foundation (grant number 00240121), and Tutkijat Maailmalle (grant number 20240032).

■ REFERENCES

(1) Hill, C. A. S. *Wood Modification: Chemical, Thermal and Other Processes*; John Wiley & Sons, Ltd., 2006.

(2) Candelier, K.; Thevenon, M.-F.; Petrissans, A.; Dumarcay, S.; Gerardin, P.; Petrissans, M. Control of Wood Thermal Treatment and Its Effects on Decay Resistance: A Review. *Ann. For Sci.* **2016**, *73* (3), 571−583.

(3) Sandberg, D.; Kutnar, A.; Mantanis, G. Wood Modification Technologies - a Review. *iForest* **2017**, *10* (6), 895.

(4) Jančíková, V.; Jablonský, M. Thermal Modification of Wood—A Review. *Sustain Chem.* **2025**, *6* (3), 19.

(5) González-Peña, M. M.; Curling, S. F.; Hale, M. D. C. On the Effect of Heat on the Chemical Composition and Dimensions of Thermally-Modified Wood. *Polym. Degrad. Stab.* **2009**, *94* (12), 2184−2193.

(6) Tjeerdsma, B. F.; Boonstra, M.; Pizzi, A.; Tekely, P.; Militz, H. Characterisation of Thermally Modified Wood: Molecular Reasons for Wood Performance Improvement. *Holz Roh Werkst* **1998**, *56* (3), 149−153.

(7) Brosse, N.; El Hage, R.; Chaouch, M.; Pétrissans, M.; Dumarçay, S.; Gérardin, P. Investigation of the Chemical Modifications of Beech Wood Lignin during Heat Treatment. *Polym. Degrad. Stab.* **2010**, *95* (9), 1721−1726.

(8) Lourenço, A.; Araújo, S.; Gominho, J.; Pereira, H.; Evtuguin, D. Structural Changes in Lignin of Thermally Treated Eucalyptus Wood. *J. Wood Chem. Technol.* **2020**, *40* (4), 258−268.

(9) Hou, S.; Wang, J.; Yin, F.; Qi, C.; Mu, J. Moisture Sorption Isotherms and Hysteresis of Cellulose, Hemicelluloses and Lignin Isolated from Birch Wood and Their Effects on Wood Hygroscopicity. *Wood Sci. Technol.* **2022**, *56*, 1087.

(10) Altgen, M.; Kyyrö, S.; Paajanen, O.; Rautkari, L. Resistance of Thermally Modified and Pressurized Hot Water Extracted Scots Pine Sapwood against Decay by the Brown-Rot Fungus Rhodonia Placenta. *Eur. J. Wood Prod* **2020**, *78* (1), 161−171.

(11) Altgen, M.; Willems, W.; Hosseinpourpia, R.; Rautkari, L. Hydroxyl Accessibility and Dimensional Changes of Scots Pine Sapwood Affected by Alterations in the Cell Wall Ultrastructure during Heat-Treatment. *Polym. Degrad. Stab.* **2018**, *152*, 244−252.

(12) Altgen, M.; Hofmann, T.; Militz, H. Wood Moisture Content during the Thermal Modification Process Affects the Improvement in Hygroscopicity of Scots Pine Sapwood. *Wood Sci. Technol.* **2016**, *50* (6), 1181−1195.

(13) Rautkari, L.; Hill, C. A. S.; Curling, S.; Jalaludin, Z.; Ormondroyd, G. What Is the Role of the Accessibility of Wood Hydroxyl Groups in Controlling Moisture Content? *J. Mater. Sci.* **2013**, *48* (18), 6352−6356.

(14) Repellin, V.; Guyonnet, R. Evaluation of Heat-Treated Wood Swelling by Differential Scanning Calorimetry in Relation to Chemical Composition. *Holzforschung* **2005**, *59* (1), 28−34.
(15) Hill, C.; Altgen, M.; Rautkari, L. Thermal Modification of Wood—a Review: Chemical Changes and Hygroscopicity. *J. Mater. Sci.* **2021**, *56*, 6581.
(16) Ringman, R.; Beck, G.; Pilgård, A. The Importance of Moisture for Brown Rot Degradation of Modified Wood: A Critical Discussion. *Forests* **2019**, *10* (6), 522.
(17) Ringman, R.; Pilgård, A.; Brischke, C.; Richter, K. Mode of Action of Brown Rot Decay Resistance in Modified Wood: A Review. *Holzforschung* **2014**, *68* (2), 239−246.
(18) Thybring, E. E. The Decay Resistance of Modified Wood Influenced by Moisture Exclusion and Swelling Reduction. *Int. Biodeter Biodegrad* **2013**, *82*, 87−95.
(19) Zelinka, S. L.; Ringman, R.; Pilgård, A.; Thybring, E. E.; Jakes, J. E.; Richter, K. The Role of Chemical Transport in the Brown-Rot Decay Resistance of Modified Wood. *Int. Wood Prod J.* **2016**, *7* (2), 66−70.
(20) Ringman, R.; Pilgård, A.; Kölle, M.; Brischke, C.; Richter, K. Effects of Thermal Modification on Postia Placenta Wood Degradation Dynamics: Measurements of Mass Loss, Structural Integrity and Gene Expression. *Wood Sci. Technol.* **2016**, *50* (2), 385−397.
(21) Belt, T.; Harju, A.; Kilpeläinen, P.; Venäläinen, M. Fungal Degradation of Extractives Plays an Important Role in the Brown Rot Decay of Scots Pine Heartwood. *Front Plant Sci.* **2022**, *13*, No. 912555.
(22) Belt, T.; Awais, M. Progressive Degradation of Acetylated Wood by the Brown Rot Fungi Coniophora Puteana and Rhodonia Placenta. *Wood Sci. Technol.* **2025**, *59*, 13.
(23) Beck, G.; Thybring, E. E.; Thygesen, L. G. Brown-Rot Fungal Degradation and de-Acetylation of Acetylated Wood. *Int. Biodeter Biodegrad* **2018**, *135*, 62−70.
(24) Thygesen, L. G.; Beck, G.; Nagy, N. E.; Alfredsen, G. Cell Wall Changes during Brown Rot Degradation of Furfurylated and Acetylated Wood. *Int. Biodeter Biodegrad* **2021**, *162*, No. 105257.
(25) Belt, T.; Harju, A.; Venäläinen, M.; Kilpeläinen, P. Fate of Organic Solvent-Soluble Extractives and Arabinogalactan during Brown Rot Degradation of Siberian Larch Heartwood. *Eur. J. Wood Prod* **2024**, *82*, 2203.
(26) Belt, T.; Altgen, M.; Awais, M.; Nopens, M.; Rautkari, L. Degradation by Brown Rot Fungi Increases the Hygroscopicity of Heat-Treated Wood. *Int. Biodeter Biodegrad* **2024**, *186*, No. 105690.
(27) Belt, T.; Awais, M.; Mäkelä, M. Chemical Characterization and Visualization of Progressive Brown Rot Decay of Wood by Near Infrared Imaging and Multivariate Analysis. *Front Plant Sci.* **2022**, *13*, No. 940745.
(28) Mäkelä, M.; Altgen, M.; Belt, T.; Rautkari, L. Hyperspectral Imaging and Chemometrics Reveal Wood Acetylation on Different Spatial Scales. *J. Mater. Sci.* **2021**, *56* (8), 5053−5066.
(29) Mäkelä, M.; Geladi, P.; Rissanen, M.; Rautkari, L.; Dahl, O. Hyperspectral near Infrared Image Calibration and Regression. *Anal. Chim. Acta* **2020**, *1105*, 56−63.
(30) Wold, S.; Esbensen, K.; Geladi, P. Principal Component Analysis. *Chemometr Intell Lab Syst* **1987**, *2* (1), 37−52.
(31) Amigo, J. M.; Grassi, S. Configuration of Hyperspectral and Multispectral Imaging Systems. In *Data Handling in Science and Technology*; Amigo, J. M., Ed.; Hyperspectral Imaging; Elsevier, 2019; Vol. *32*, pp 17−34; DOI: 10.1016/B978-0-444-63977-6.00002-X.
(32) Savitzky, A.; Golay, M. J. E. Smoothing and Differentiation of Data by Simplified Least Squares Procedures. *Anal. Chem.* **1964**, *36* (8), 1627−1639.
(33) Smilde, A. K.; Jansen, J. J.; Hoefsloot, H. C. J.; Lamers, R.-J. A. N.; van der Greef, J.; Timmerman, M. E. ANOVA-Simultaneous Component Analysis (ASCA): A New Tool for Analyzing Designed Metabolomics Data. *Bioinformatics* **2005**, *21* (13), 3043−3048.
(34) Levä, T.; Mahlamäki, E.; Kosourov, S.; Allahverdiyeva, Y.; Mäkelä, M.; Tammelin, T. Non-Invasive Monitoring of Cyanobacteria Growth in a Nanocellulose Matrix. *Algal Res.* **2025**, *89*, No. 104090.
(35) Zwanenburg, G.; Hoefsloot, H. C. J.; Westerhuis, J. A.; Jansen, J. J.; Smilde, A. K. ANOVA−Principal Component Analysis and ANOVA−Simultaneous Component Analysis: A Comparison. *Journal of Chemometrics* **2011**, *25* (10), 561−567.
(36) Vis, D. J.; Westerhuis, J. A.; Smilde, A. K.; van der Greef, J. Statistical Validation of Megavariate Effects in ASCA. *BMC Bioinformatics* **2007**, *8* (1), 322.
(37) de Jong, S. SIMPLS: An Alternative Approach to Partial Least Squares Regression. *Chemometr Intell Lab Syst* **1993**, *18* (3), 251−263.
(38) Chong, I.-G.; Jun, C.-H. Performance of Some Variable Selection Methods When Multicollinearity Is Present. *Chemometr Intell Lab Syst* **2005**, *78* (1), 103−112.
(39) Holtman, K. M.; Chang, H.; Jameel, H.; Kadla, J. F. Quantitative 13C NMR Characterization of Milled Wood Lignins Isolated by Different Milling Techniques. *J. Wood Chem. Technol.* **2006**, *26* (1), 21−34.
(40) Goundalkar, M. J.; Corbett, D. B.; Bujanovic, B. M. Comparative Analysis of Milled Wood Lignins (MWLs) Isolated from Sugar Maple (SM) and Hot-Water Extracted Sugar Maple (ESM). *Energies* **2014**, *7* (3), 1363−1375.
(41) Ralph, J.; Landucci, L. L. NMR of Lignins. In *Lignin and lignans: advances in chemistry:*; Heitner, C., Dimmel, D., Schmidt, J.,, Eds.; CRC Press: Boca Raton, 2010; pp 138−246.
(42) Lancefield, C. S.; Wienk, H. L. J.; Boelens, R.; Weckhuysen, B. M.; Bruijnincx, P. C. A. Identification of a Diagnostic Structural Motif Reveals a New Reaction Intermediate and Condensation Pathway in Kraft Lignin Formation. *Chem. Sci.* **2018**, *9* (30), 6348−6360.
(43) Sette, M.; Wechselberger, R.; Crestini, C. Elucidation of Lignin Structure by Quantitative 2D NMR. *Chem.—Eur. J.* **2011**, *17* (34), 9529−9535.
(44) Chaouch, M.; Dumarçay, S.; Pétrissans, A.; Pétrissans, M.; Gérardin, P. Effect of Heat Treatment Intensity on Some Conferred Properties of Different European Softwood and Hardwood Species. *Wood Sci. Technol.* **2013**, *47* (4), 663−673.
(45) Metsä-Kortelainen, S.; Viitanen, H. Decay Resistance of Sapwood and Heartwood of Untreated and Thermally Modified Scots Pine and Norway Spruce Compared with Some Other Wood Species. *Wood Mater. Sci. Eng.* **2009**, *4* (3−4), 105−114.
(46) Welzbacher, C. R.; Rapp, A. O. Durability of Thermally Modified Timber from Industrial-Scale Processes in Different Use Classes: Results from Laboratory and Field Tests. *Wood Mater. Sci. Eng.* **2007**, *2* (1), 4−14.
(47) Fackler, K.; Schwanninger, M. Polysaccharide Degradation and Lignin Modification during Brown Rot of Spruce Wood: A Polarised Fourier Transform near Infrared Study. *J. Near Infrared Spectrosc* **2010**, *18* (6), 403−416.
(48) Schwanninger, M.; Rodrigues, J. C.; Fackler, K. A Review of Band Assignments in near Infrared Spectra of Wood and Wood Components. *J. Near Infrared Spectrosc* **2011**, *19* (5), 287−308.
(49) Popescu, C.-M.; Popescu, M.-C. A near Infrared Spectroscopic Study of the Structural Modifications of Lime (Tilia Cordata Mill.) Wood during Hydro-Thermal Treatment. *Spectrochim Acta A Mol. and Biomol Spectrosc* **2013**, *115*, 227−233.
(50) Jochemsen, A.; Alfredsen, G.; Burud, I. Hyperspectral Imaging as a Tool for Profiling Basidiomycete Decay of Pinus Sylvestris L. *Int. Biodeter Biodegrad* **2022**, *174*, No. 105464.
(51) King, J. F.; Vig, B. Near-Infrared Spectra of Aliphatic Aldehydes. *Can. J. Chem.* **1962**, *40* (5), 1023−1025.
(52) Powers, R. M.; Harper, J. L.; Tai, H. Determination of Aromatic Aldehydes by Near-Infrared Spectrophotometry. *Anal. Chem.* **1960**, *32* (10), 1287.
(53) Nuopponen, M.; Vuorinen, T.; Jämsä, S.; Viitaniemi, P. Thermal Modifications in Softwood Studied by FT-IR and UV Resonance Raman Spectroscopies. *J. Wood Chem. Technol.* **2005**, *24* (1), 13−26.

(54) Tjeerdsma, B.; Militz, H. Chemical Changes in Hydrothermal Treated Wood: FTIR Analysis of Combined Hydrothermal and Dry Heat-Treated Wood. *Holz Roh Werkst* **2005**, *63*, 102−111.
(55) Yildiz, S.; Gümüşkaya, E. The Effects of Thermal Modification on Crystalline Structure of Cellulose in Soft and Hardwood. *Build Environ* **2007**, *42* (1), 62−67.
(56) Curling, S. F.; Clausen, C. A.; Winandy, J. E. Relationships between Mechanical Properties, Weight Loss, and Chemical Composition of Wood during Incipient Brown-Rot Decay. *Forest Prod J.* **2002**, *52*, 34−40.
(57) Kaffenberger, J. T.; Schilling, J. S. Comparing Lignocellulose Physiochemistry after Decomposition by Brown Rot Fungi with Distinct Evolutionary Origins. *Environ. Microbiol* **2015**, *17* (12), 4885−4897.
(58) Filley, T. R.; Cody, G. D.; Goodell, B.; Jellison, J.; Noser, C.; Ostrofsky, A. Lignin Demethylation and Polysaccharide Decomposition in Spruce Sapwood Degraded by Brown Rot Fungi. *Org. Geochem.* **2002**, *33* (2), 111−124.
(59) Jin, L.; Schultz, T. P.; Nicholas, D. D. Structural Characterization of Brown-Rotted Lignin. *Holzforschung* **1990**, *44* (2), 133−138.
(60) Rese, M.; van Erven, G.; Veersma, R. J.; Alfredsen, G.; Eijsink, V. G. H.; Kabel, M. A.; Tuveng, T. R. Detailed Characterization of the Conversion of Hardwood and Softwood Lignin by a Brown-Rot Basidiomycete. *Biomacromolecules* **2025**, *26*, 1063.
(61) Sun, Q.-N.; Qin, T.-F.; Li, G.-Y. Chemical Groups and Structural Characterization of Brown-Rotted Pinus Massoniana Lignin. *Int. J. Polym. Anal Ch* **2009**, *14* (1), 19−33.
(62) Yelle, D. J.; Wei, D.; Ralph, J.; Hammel, K. E. Multidimensional NMR Analysis Reveals Truncated Lignin Structures in Wood Decayed by the Brown Rot Basidiomycete Postia Placenta. *Environ. Microbiol* **2011**, *13* (4), 1091−1100.
(63) Martínez, A. T.; Rencoret, J.; Nieto, L.; Jiménez-Barbero, J.; Gutiérrez, A.; del Río, J. C. Selective Lignin and Polysaccharide Removal in Natural Fungal Decay of Wood as Evidenced by in Situ Structural Analyses. *Environ. Microbiol* **2011**, *13* (1), 96−107.
(64) Kim, J.-Y.; Hwang, H.; Oh, S.; Kim, Y.-S.; Kim, U.-J.; Choi, J. W. Investigation of Structural Modification and Thermal Characteristics of Lignin after Heat Treatment. *Int. J. Biol. Macromol.* **2014**, *66*, 57−65.

https://doi.org/10.1021/acssuschemeng.5c08352
ACS Sustainable Chem. Eng. 2025, 13, 17050−17060